

Fatigue Crack Growth Mechanisms in Ti6242 Lamellar Microstructures: Influence of Loading Frequency and Temperature

F. SANSOZ and H. GHONEM

Fatigue crack growth experiments were carried out on Ti6242 alloy with large colony size. The alloy was heat treated to provide three different lamella size; fine, coarse, and extra coarse. Tests were conducted at two temperatures, 520 °C and 595 °C, using two loading frequencies, 10 and 0.05 Hz. The latter frequency was examined with and without a 300-second hold time. All tests were performed in air environment and at a stress ratio of 0.1. This study shows that at 520 °C, the Fatigue crack growth rate (FCGR) is not significantly influenced by changes in the microstructure. For 0.05 Hz/low ΔK , however, the FCGR is higher in the fine lamellar microstructure and is accompanied by the appearance of a plateau, which disappears in the extra large lamella microstructure. Furthermore, the addition of a 300-second hold time does not alter the crack growth rate. At 595 °C, while the general level of the FCGR is higher than that at 520 °C, the effects of loading frequency and hold time remain similar to those reported at the lower temperature. Unlike the results at 520 °C, however, the FCGR at low ΔK is not influenced by variations in lamellar microstructure. Under all test conditions, the fatigue process is predominantly controlled by one single mechanism associated with transcolony fracture and formation of quasi-cleavage facets. The fatigue crack growth results and the associated fracture behavior as obtained in this study are correlated to the crack-tip shear activity and transmission at the α/β interfaces. A general hypothesis accounting for the role of loading frequency, temperature, and microstructure on the observed cracking mechanisms is presented.

I. INTRODUCTION

THE α/β and near- α titanium alloys are widely used in commercial and military aeroengines.^[1] In the past decades, a considerable amount of research has been conducted on these materials with the objective of fully exploiting their high-temperature potential. A number of investigations have succeeded in relating the details of the processing route to the mechanical properties at elevated temperatures.^[2,3] A particular advance in that domain is the processing of fully lamellar microstructures, made of colonies of similarly aligned α/β platelets within large prior- β grains, which promote lower creep strain and better long fatigue crack growth behavior than any other titanium microstructures.^[4,5,6] While several attempts have been carried out to understand the influence of the microstructure features on the mechanical properties, discrepancies exist concerning the nature of creep-fatigue interactions in the crack growth behavior of lamellar microstructures.

It is acknowledged that the fatigue crack growth (FCG) process at elevated temperature is a complex interaction between loading frequency, temperature, microstructure, and environment.^[7,8] Earlier investigations have demonstrated that the loading frequency and hold time at maximum load have an influence on the fatigue crack growth rate (FCGR) of Ti alloys at elevated temperature. The crack growth rate

is reported to be inversely proportional to the loading frequency.^[9] In near- α alloy Ti-1100, the introduction of 300-second hold time periods at peak stress also causes a transition from low to high crack growth rate,^[10,11,12] being accompanied by a change in the fracture mode from quasi-cleavage to intergranular fracture. Lesterlin *et al.*^[13] have observed that in Ti6246 alloy, the frequency influence is much more pronounced at temperatures above 465 °C. In that study, hold time also produced intergranular fracture, but the effect on the crack growth rates saturates for hold times higher than 100 seconds. The role of temperature observed by these authors is consistent with the results of earlier works^[14,15] on the creep resistance of Ti6211 and Ti6242 alloys at elevated temperature. In these alloys, there is a critical temperature (482 °C) below which the activation energy for creep is associated with oxygen diffusion in α titanium phase. At higher temperature with higher activation energies, self-diffusion overtakes the effects of oxygen diffusion. In addition, Miller *et al.*^[14] have observed that fracture mechanisms in basketweave microstructures at 550 °C occur typically by microvoid formation and sliding at the α layer of prior β grains. This result, coupled with the studies discussed previously, supports the assumption that the FCG process of Ti alloys at elevated temperatures is governed by creep-fatigue interactions. At identical temperature, Miller *et al.*^[14] have observed, however, that the fracture mode becomes strongly different if the microstructure is fully lamellar; creep rupture being controlled by void formation and sliding at α/β interfaces between the platelets within the prior β grains. Several investigations in fully lamellar microstructures have also shown that a common feature of high-temperature fracture surfaces is the presence of large transgranular facets at low ΔK value and striations and

F. SANSOZ, Postdoctor, is with the Department of Mechanical Engineering, The Johns Hopkins University, Baltimore, MD 21218. H. GHONEM, Professor, is with the Department of Mechanical Engineering, The University of Rhode Island, Kingston, RI 02881. Contact e-mail: ghonem@egr.uri.edu

Manuscript submitted May 28, 2002.

dimple formations at higher ΔK values.^[7,16] It is believed that microstructure variations have an important role in affecting hold time sensitivity and highly contribute to the large amount of inconsistencies raised from the experimental results.^[17] In titanium lamellar microstructures, the presence of a hold time at peak stress has been noticed to produce an increase in both fatigue crack growth rates^[18,19] and same crack growth rates,^[20,21] or even a decrease in crack growth rates.^[22,23] The study of Stubbington and Pearson,^[24] who observed no hold time effect in textured microstructures when the crack propagated normal to the basal plane of the α phase and a large effect when the basal plane coincided with the plane of maximum stress, suggests also that a close interaction between the microstructure and high-temperature effects exists in fully lamellar titanium alloys.

The relative importance of different microstructure features in the FCG process of lamellar titanium alloys has not provided a general hypothesis. For example, it is assumed that the colony boundaries are a major barrier to slip due to easy transmission between α phase and β phase.^[25] In this view, the effective length of a slip band in an activated system would govern the evolution rate of the corresponding damage process. This view is supported by observations indicating that the strength of a microstructure tends to increase as the colony size decreases.^[4,14,26] Ravichandran,^[27] however, concluded that α platelets are dominant in fully lamellar microstructures, while colonies are important in basketweave structures. Otherwise, separate studies have focused on the role played by α/β interfaces in inhibiting some of the slip systems. Chan *et al.*^[28] studied the deformation of individual aligned colonies in compression and demonstrated that the yield stress of the colony was controlled by the angle between the slip direction and the α/β interface. The yield stress was at its lowest when the slip direction was parallel to the interface. Suri *et al.*,^[29] in their work on single-colony crystals of Ti-5-2.5-0.5 alloys, have shown that an anisotropy in mechanical properties exists between the different slip systems transmitted at α/β interfaces, when subjected to room-temperature creep. The correlation of these observations to polycrystalline alloys, however, is worthy of further investigations. Moreover, no attempt has been made before in α/β titanium lamellar microstructures to rationalize the FCG mechanisms in terms of crack-tip slip transmission at interfaces.

The current study explores the crack-tip damage process in α/β Ti lamellar microstructures and its interaction with the loading frequency and temperature. For that purpose, FCG tests are performed at elevated temperatures on a commercial α/β titanium alloy, Ti-6Al-2Sn-4Zr-2Mo-0.1Si (Ti6242), with three lamellar microstructures varying in their lamella size and colony size. All tests are carried out at a typical service temperature, 520 °C, and at higher temperature, 595 °C, using two different loading frequencies: 0.05 and 10 Hz. The effect of a 300 second hold time at peak stress is also addressed at 0.05 Hz. The first part of the article presents the experimental procedure used for the FCG testing. This includes the description of the heat-treatment route conducted on the microstructures of this study. The results of the fatigue tests obtained in terms of crack growth rates and associated fracture mechanisms are then presented and commented through Scanning electron microscopy (SEM) examinations. The last part discusses the significance

of loading frequency, temperature, and microstructure in the controlling crack growth process and its relationship with the crack-tip slip transmission at α/β interfaces.

II. EXPERIMENTAL PROCEDURE

The material used in this study was manufactured for compressor disks forged at 30 °C above the β transus (995 °C). Its chemical composition is Ti—balance, Al—6.000, Sn—1.940, Zr—4.095, Mo—2.045, Si—0.115, Fe—0.031, C—0.009, and O—0.011 (in wt pct). The as-received microstructure corresponds to an arrangement of small α/β lamellar colonies bordered by larger prior β grains. A series of solutioning treatments was carried out in order to change the size of the features of this microstructure. The samples were encapsulated within a quartz tube and maintained at high vacuum atmosphere using a dynamic pumping system during the heat treatment. The temperature of heat treatment was monitored within the tube through thermocouple measurements with accuracy greater than 2 °C. The typical heat treatment is a solutioning treatment at 1025 °C for 1 hour followed by quenching at room temperature. In this quenching process, the specimens were left under vacuum inside the quartz tube. Thermal stabilization, as well as strengthening of the microstructure, was ensured by precipitation of α_2 (Ti₃Al) particles using a conventional aging treatment. This aging treatment is carried out at 595 °C for 8 hours in a vacuum environment followed by quenching at ambient atmosphere using the quenching procedure described previously. In Ti alloys, the temperature of solutioning controls the size of the prior β grains. For the Ti6242 alloy, however, the size of this feature becomes very large (>0.5 mm) after reaching the β transus. The influence of the solutioning temperature, therefore, was not investigated, since there was no possibility of reaching a small prior β grain size by conventional treatment. Particular attention was paid, however, to the aspects of the α platelets and the α/β colonies. It is known that the size of these features depends on the cooling rate of quenching after the solutioning treatment; the platelets and colony dimension increase as the cooling rate decreases.^[4] Three different cooling rates were imposed: air-cooling (134 °C/min), furnace cooling (10 °C/min), and very slow furnace cooling (1 °C/min). The resulting microstructures are shown in Figure 1. Microscopic examinations were carried out using both SEM and optical microscopy. Quantitative measurements were conducted on each microstructure in order to determine the average diameter of prior β grains and α/β colonies, as well as the thickness of α and β platelets. The diameter of prior β grain and α/β colony was measured using the mean intercept method over 20 features of each type. The thickness of α and β platelets was estimated by taking the average distance over ten platelets measured in different colonies. These results are reported in Figure 2 as a function of the cooling rate. Figure 2(a) shows that the size of the prior- β grains is kept relatively large (0.8 mm). The cooling rate is also shown to have a significant effect on the dimension of the α/β colony and the α platelets (Figures 2(a) and 3(b), respectively). The three microstructures tested in this work will be referred to as fine lamellar, coarse lamellar, and extra-coarse lamellar microstructures. The average dimension of α platelets, in each of these microstructures, is 0.7, 2.0, and 5.9 μm , respectively.

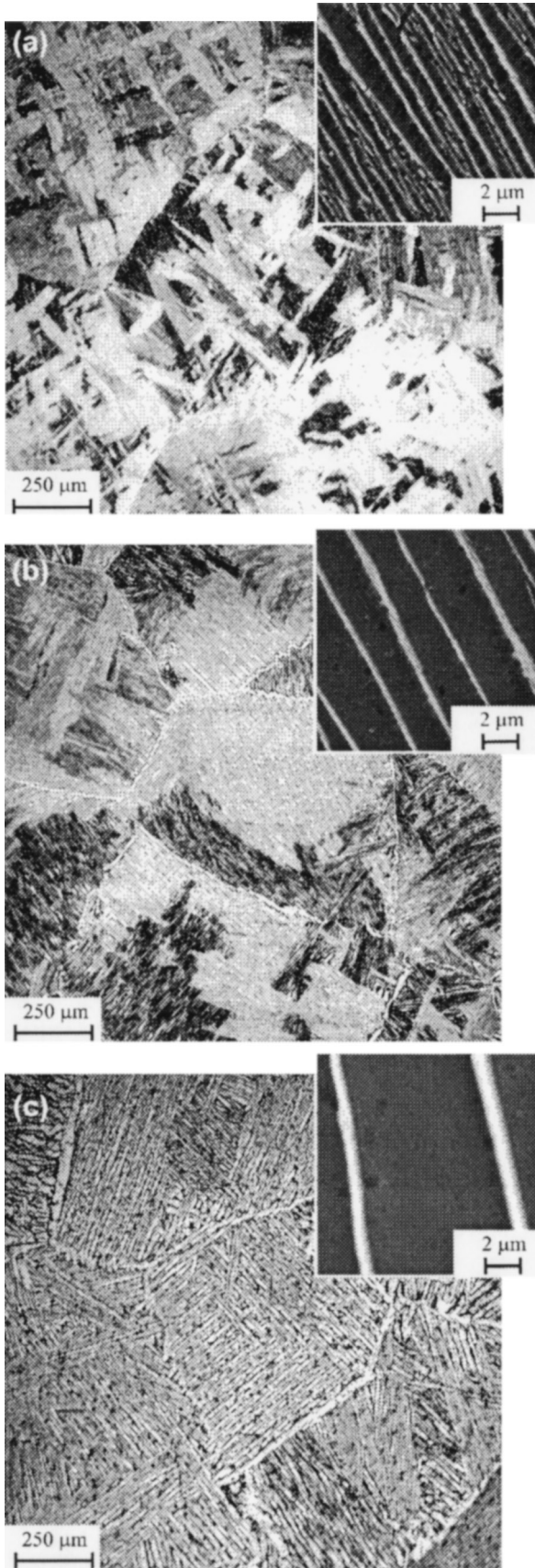


Fig. 1—Ti6242 microstructures: (a) fine lamellar, (b) coarse lamellar, and (c) extra-coarse lamellar.

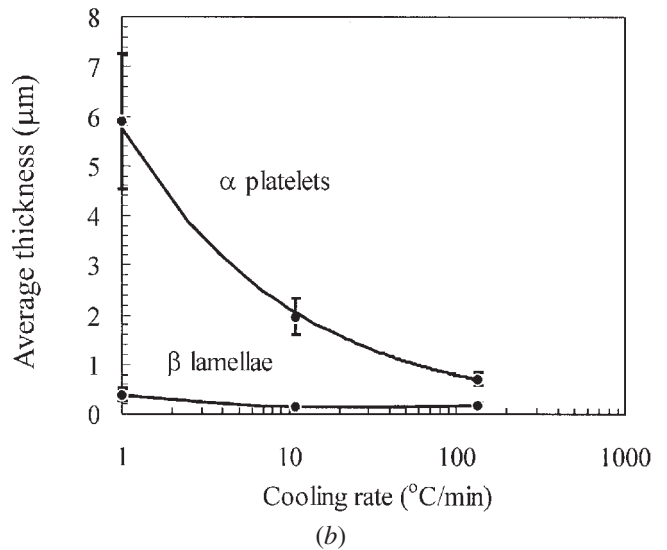
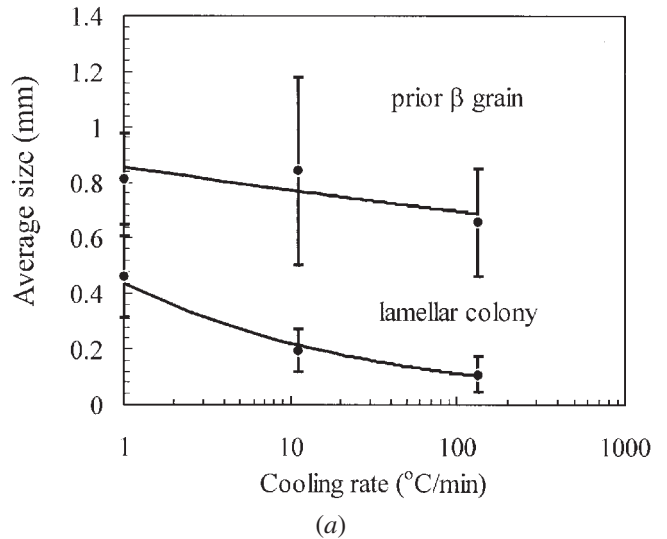


Fig. 2—(a) and (b) Average size of microstructure features related to the three microstructures presented in Fig. 1, as a function of the cooling rate imposed after solutioning treatment.

The average size of the β lamellas is found to be similar in all produced microstructures, and equal to $0.2 \mu\text{m}$, as shown in Figure 2(b).

Fatigue crack growth experiments were conducted using compact tension specimens ($B = 6.35 \text{ mm}$ and $W = 25.4 \text{ mm}$) made of the three microstructures presented previously. Prior to testing, the specimen surfaces were ground mechanically up to 800 grit, then with diamond pastes down to $1 \mu\text{m}$. In order to reveal the microstructure on the crack path, the polished surfaces were etched by immersing the specimen in Kroll's reagent for 10 seconds. A room-temperature precracking was performed at a loading frequency of 20 Hz to obtain an initial crack length of $a_0 = 0.3 W$. The crack growth was measured using optical measurements made on the two sides of the test specimen. In addition, the crack growth was monitored using the potential difference method. The potential difference curve used in these experiments was calibrated on the basis of optical

measurements. All FCG tests were conducted on servohydraulic material testing systems controlled by a Test Star IIS (MTS Systems Corporation, Eden Prairie, MN) computer system. Heating of the specimens was achieved using a clamshell furnace in which the specimen temperature is controlled by two thermocouples spot-welded on two opposite corners of the top and bottom surfaces of the specimen. In this way, temperature variations in all tests were maintained less than 5 °C along the height and width of the specimen. Tests were conducted at two temperatures, 520 °C and 595 °C. The crack mouth opening displacement was measured using a high-temperature clip gage. These data were used to determine the crack opening level during the test by means of the compliance method. All tests were performed with a constant load ratio $R = 0.1$. Scanning electron microscopy was used to examine the fracture surface of each specimen.

Prior to investigating the role of the loading frequency on the fatigue crack growth rate (FCGR) of the three microstructures, a preliminary FCG test was performed at 520 °C on the as-received microstructure. This test was conducted at a constant ΔK (20 MPa $\sqrt{\text{m}}$) with different loading frequencies varying from 0.01 to 10 Hz. Results of this test in Figure 3 indicate that a significant increase of crack growth rate occurs at frequencies lower than 0.1 Hz. The three microstructures mentioned previously therefore were examined by using two loading frequencies, 10 and 0.05 Hz, hereafter, referred to as high and low frequency, respectively. The latter frequency was applied with and without 300-second hold time imposed at the maximum load level to explore creep effects within the loading cycle.

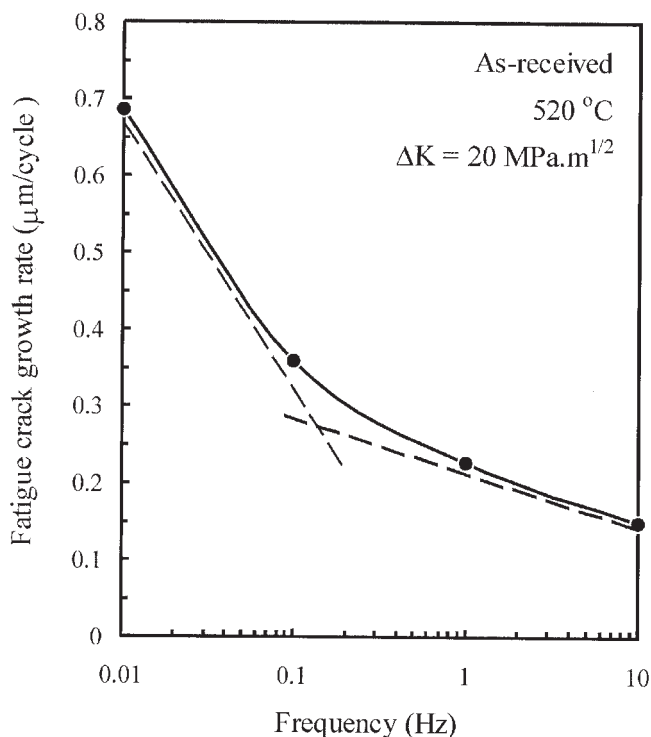


Fig. 3—Effect of loading frequency on FCGR of the as-received Ti6242 microstructure at 520 °C.

III. RESULTS

A. Fatigue Crack Growth Rates

Results of the FCGR performed on the three microstructures are first examined at 520 °C. It is shown in Figure 4 that the presence of a 300-second hold time at peak stress has no influence on these microstructures. Es-Souni^[30] has recently investigated the creep behavior of Ti6242 alloy with different microstructures at 500 °C. This author reported that lamellar microstructures exhibit very small value of primary creep strain, typically less than 0.25 times the elastic strain as compared to other microstructures of the same alloy. This suggests that the creep strain corresponding to 300-second durations is not sufficient to produce crack-tip fatigue/creep effects in lamellar Ti6242 at this temperature. On the other hand, data presented in Figure 5 show that Ti6242 alloy exhibits strong loading-rate sensitivity, the FCGR being significantly higher at low loading frequency than at high frequency. Several authors have reconciled this type of difference by accounting for the crack-tip closure effects (for example, the work of Ghonem and Foerch^[9] on Ti-1100 alloy). The crack-tip closure is generally determined by assessing the force-displacement relationship at the crack mouth during the loading part of the cycle. Using a crack mouth displacement gage, no crack closure variations were detected under the different test conditions and for the explored ΔK range, 17 to 40 MPa $\sqrt{\text{m}}$. It is concluded that the loading-rate sensitivity of Ti6242 alloy at 520 °C can-

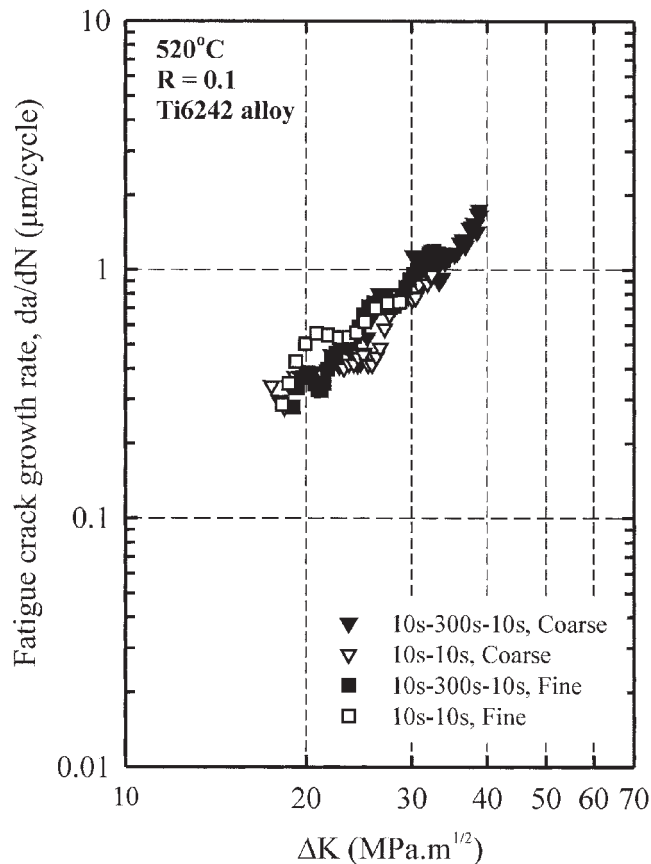


Fig. 4—Effects of 300-second dwell time at peak stress on the fatigue crack growth rate at 520 °C of coarse and fine lamellar microstructures.

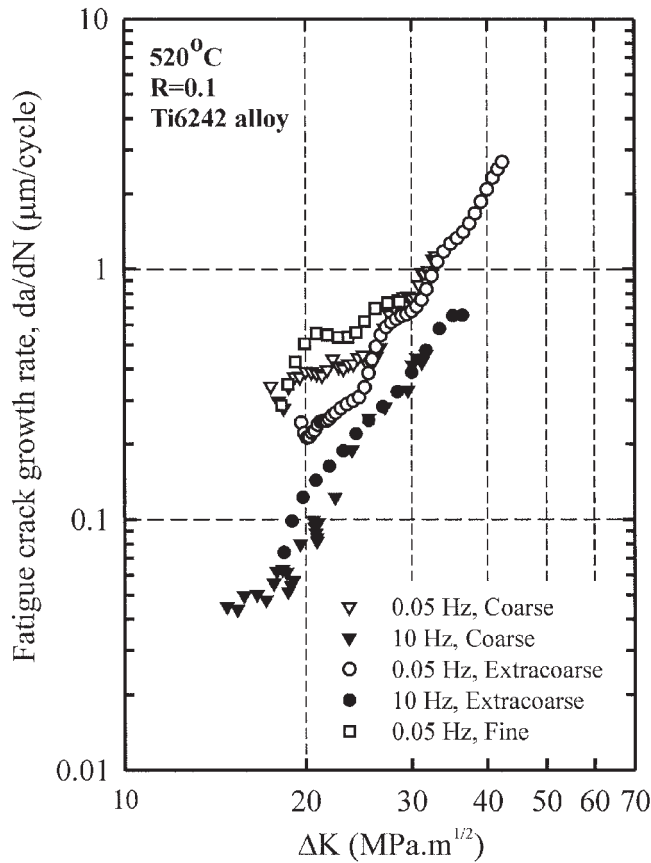


Fig. 5—Effects of loading frequency on the FCGR at 520 °C of three lamellar microstructures.

not be rationalized by taking the crack closure effect into account. Moreover, Figure 5 shows that the microstructure has little influence on the FCGR at ΔK values higher than 30 $\text{MPa}\sqrt{\text{m}}$. Differences were observed at 0.05 Hz below this ΔK level. The FCGR of the fine lamellar microstructure was found to be independent of ΔK in the early stage of propagation. This “plateau” effect, which is less pronounced in the coarse microstructure and almost absent in the extra-coarse microstructure, could be interpreted in terms of microstructure or, as suggested by other authors, related to combined microstructure/environment effects. This will be addressed in the discussion section of the paper.

Shifting attention to results obtained at 595 °C, it is observed in Figure 6 that the effects of loading frequency and hold time on the FCGR remain, to a large extent, similar to those reported at 520 °C. No noticeable changes in the crack closure levels were detected at 595 °C as a function of ΔK . One could discern, however, a slight increase in the overall FCGR at 595 °C, which was attributed to the role of temperature on the decrease of the dynamic elastic modulus.^[13,31] Furthermore, the microstructure is not influential on the FCGR, even at the early stage of propagation, where differences were detected at 520 °C. Nevertheless, one exception to this is linked to the presence of a 300-second hold time at 0.05 Hz, which shows a substantial increase of FCGR at ΔK value higher than 31 $\text{MPa}\sqrt{\text{m}}$. In addition, the ΔK values at which fracture occurred in test specimens with a hold time loading cycle are found to be

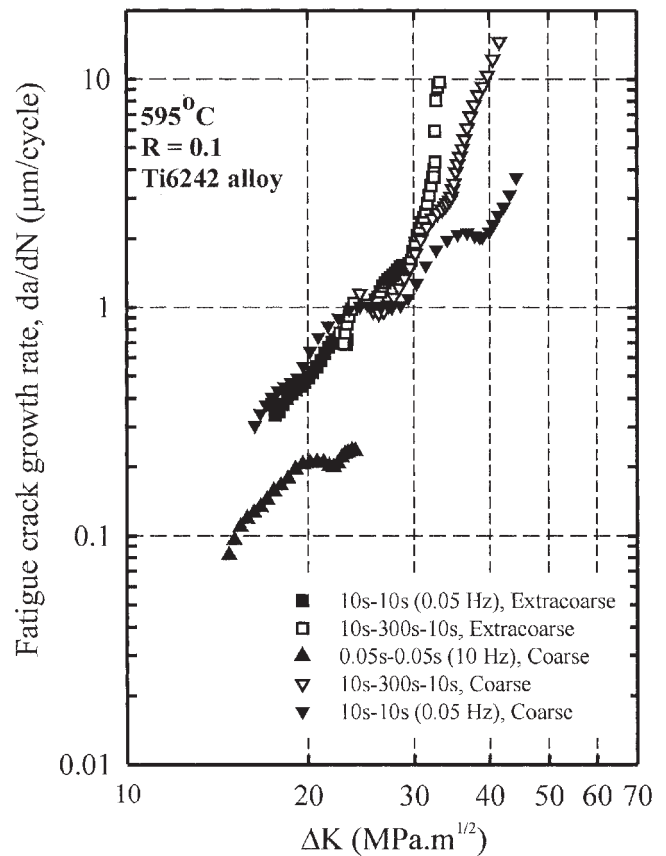


Fig. 6—Effects of 300-second dwell time and of loading frequency on the FCGR at 595 °C of three lamellar microstructures.

equal to 45 $\text{MPa}\sqrt{\text{m}}$, which is lower than that obtained in specimens tested without a hold time ($>60 \text{MPa}\sqrt{\text{m}}$). In this near-fracture toughness region, the extra-coarse lamellar microstructure seems more sensitive to hold time effects than the coarse lamellar microstructure. It is known that the fracture toughness is sensitive to the colony size of lamellar Ti alloys, particularly to the effective slip length, since the latter is more likely constrained by the colony boundaries at large applied K .^[32,33] It was known, however, that the dependence of fracture toughness on colony size could be hindered by the geometrical considerations of crack front roughness in large colony microstructures.^[4] It will be shown later in the discussion that considering the prior- β grain size instead of the colony size may provide a better means of interpreting the preceding results. To account for the differences in crack growth behavior obtained at different test conditions, further examinations of the corresponding fracture mechanisms were made. The results of these examinations are presented in Section B.

B. Fracture Surface Observations

The damage mechanisms associated with the fatigue crack growth rate curves described previously were investigated by examining the mode of failure on the specimen faces and their associated fracture surface. The surfaces display two typical fracture patterns often reported in titanium lamellar

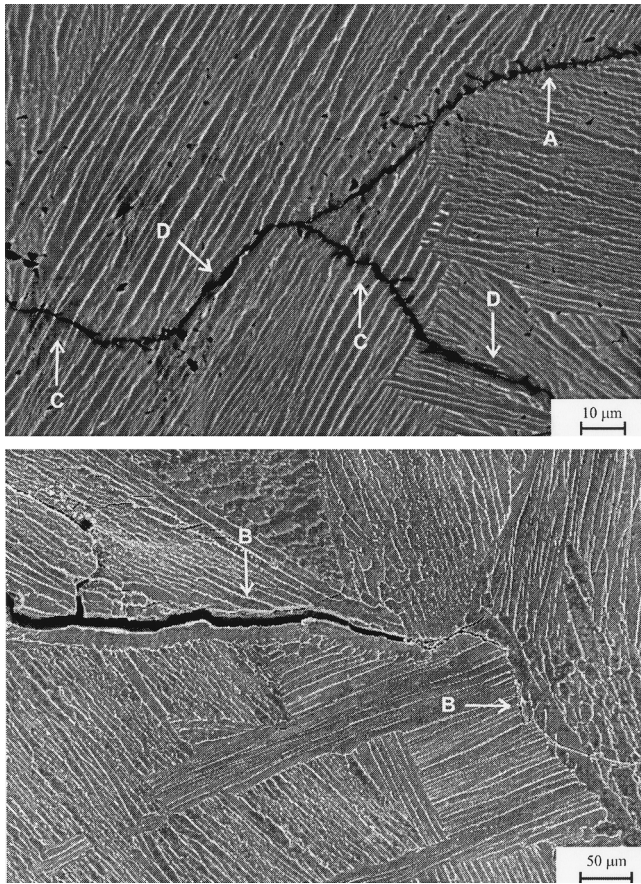


Fig. 7—The four typical fracture patterns in lamellar Ti alloys at elevated temperature: interboundary fracture (A) between α/β colonies or (B) prior β grains, and transcolony fracture (C) traversing or (D) matching the platelets long-axis orientation.

microstructures being interboundary and transcolony fractures. The interboundary fracture is related here to decohesion of intercolony boundaries or prior β grain layers. The second pattern, transcolony fracture, is referred to as crack paths either crossing the lamella or parallel to the lamellae direction. The four typical fracture patterns are shown in Figure 7.

It was undertaken to relate each of the loading and temperature conditions to one of the fracture patterns discussed previously. The region of the curves represented in Figure 6, which exhibits enhanced fatigue crack growth rates in the presence of a 300-second hold time at 595 °C, was first investigated. In this region, the final separation is observed to occur along prior β grain boundaries with the intergranular facets exhibiting large dimples (Figure 8(a)). A large number of sliding α/β interfaces occurring within the lamellar colonies was also detected in the vicinity of the intergranular crack paths, as shown in Figure 8(b). Attention is now paid to the other regions of the $d_a/dN - \Delta K$ curves represented in Figures 4 through 6. On the fracture surface corresponding to these regions, the relative percentage of transcolony and interboundary fractures was determined by examining the crack path along each fractured colony on both sides of unbroken test specimens. A total of 546 and 210 fractured colonies have been investigated after testing at 520 °C and 595 °C, respectively. Results of these exam-

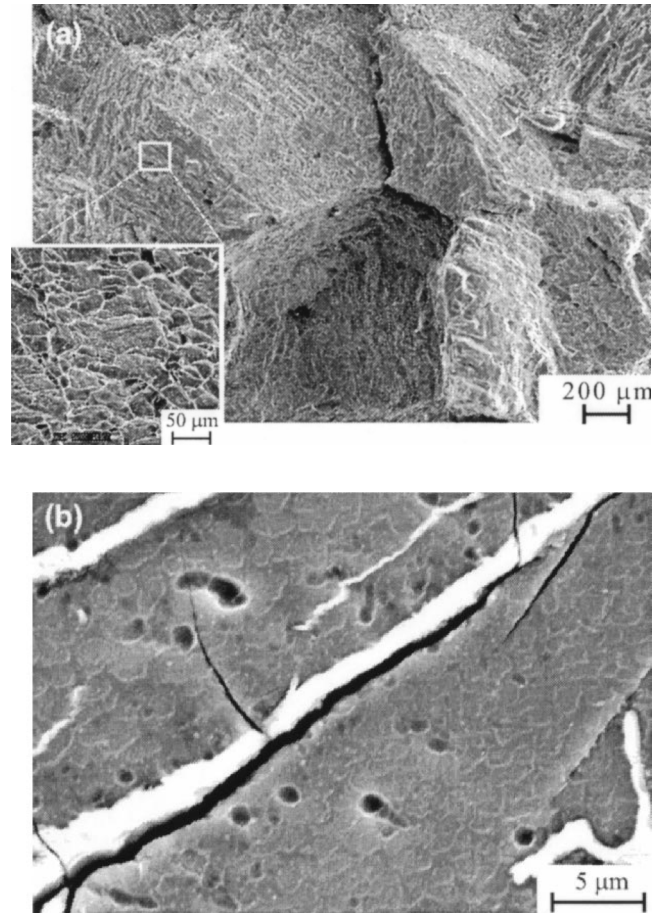


Fig. 8—Fracture appearance in the postfailure region of specimens tested at 595 °C with dwell cycles: (a) intergranular fracture accompanied by dimples and void formation on grain faces and (b) sliding and decohesion at α/β interfaces.

inations are given as a function of the loading frequency in Figure 9. It is shown that, under all test conditions, the fatigue process is predominantly controlled by one single mechanism related to transcolony fracture. In addition, it is observed on the fracture surfaces that the fracture is dominated by large planar facets at low and intermediate ΔK regions ($<40\text{MPa}\sqrt{\text{m}}$, Figure, 10(a)), while it promotes typical parallel ripple formations at higher applied ΔK values, as shown in Figure 10(b). It is important to emphasize, however, that faceting constitutes the mode of failure during most of the specimen lifetime in all testing conditions. The facet formation was observed independently of the states of stress and strain triaxiality from the interior to the surface of the specimen. This conclusion, coupled with observations showing that the crack front curvature did not vary during the crack propagation, suggests that bulk and surface fracture mechanisms are not significantly different. The dimension of the transcolony facets was found to be similar to the α/β colony size, and their plane tends to be oriented along heavily sheared bands, which gives credence for quasi-cleavage facets. Furthermore, it is observed that the deformation is highly heterogeneous in the vicinity of the shear plane, at both 520 °C and 595 °C, but apparently confined within a single colony ahead of the crack tip, as shown in Figure 11.

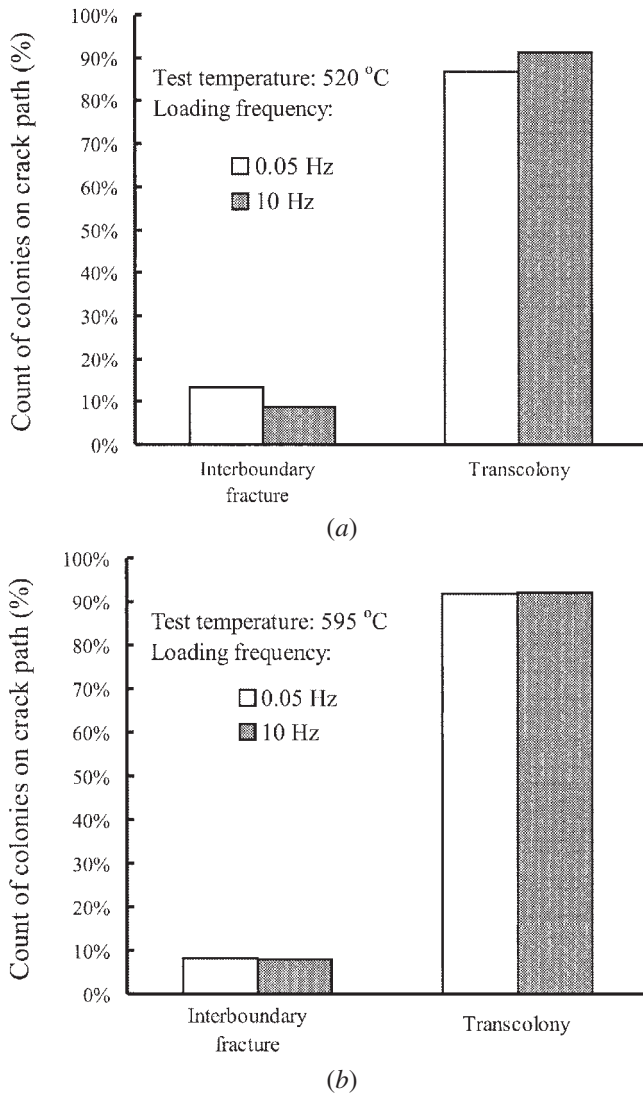


Fig. 9—Effects of loading frequency on the percentage of transcolony and interboundary colonies crossing the crack path at (a) 520 °C and (b) 595 °C.

In order to detect a preferential direction for quasi-cleavage with respect to the colony orientation, the angle between the planar crack path and the long axis direction of fractured colonies has been measured. These results are represented in Figure 12. In this figure, we emphasized for all test conditions the relative percentage of near-0 deg and near-90 deg angles. These two angles of primary interest correspond to either parallel or transverse crack paths, respectively, with respect to the long axis direction of the α platelets. It is important to note that in the case of parallel-to-lamella crack path, the failure process occurs within the α phase with no apparent α/β interface sliding. Results represented in Figure 12(a) suggest that, at 10 Hz and 520 °C, an equal tendency for parallel and transverse cracking exists. On the other hand, a decrease of the loading frequency to 0.05 Hz leads to a significant reduction for transverse crack paths and predominance for parallel crack paths (Figure 11(b)). At 595 °C, both low and high loading frequencies exhibit near-0 deg and near-90 deg crack paths, suggesting that the crack path selectivity observed at 520 °C as a function of the loading frequency is almost absent at this temperature.

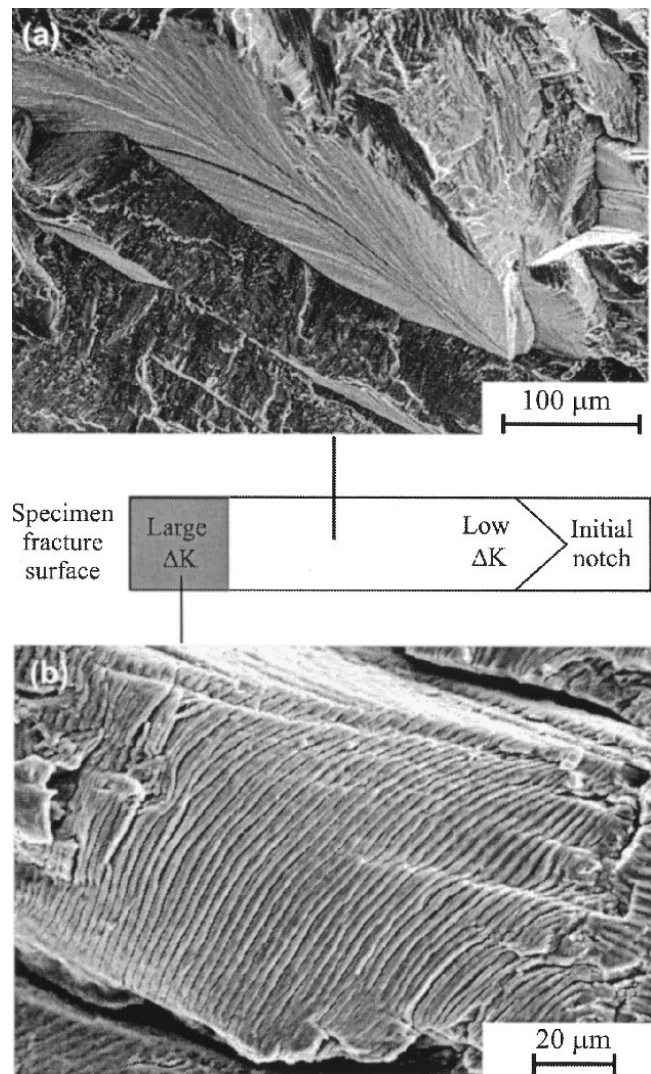


Fig. 10—Typical fracture mode transition from (a) quasi-cleavage planar facets at low ΔK to (b) ductile ripple appearance. Note that striation marks are only observed in the very last stage of crack propagation.

The results described previously coupled with the observations of quasi-cleavage facets, would suggest that an analysis of the slip process might provide a means to re-examine and rationalize the reported crack growth rates and associated fracture path. Discussions on the interactions between loading frequency, temperature, and shear processes are given in Section IV.

IV. DISCUSSION

A. Slip Behavior

The specific trends of the slip processes for given conditions of loading and temperature are made by examining the corresponding dislocation arrangements *via* the use of transmission electron microscopy. For planar slip, however, a general view can be identified through the slip traces left on the specimen surface after the fracture events took place. These traces were determined in the present study using

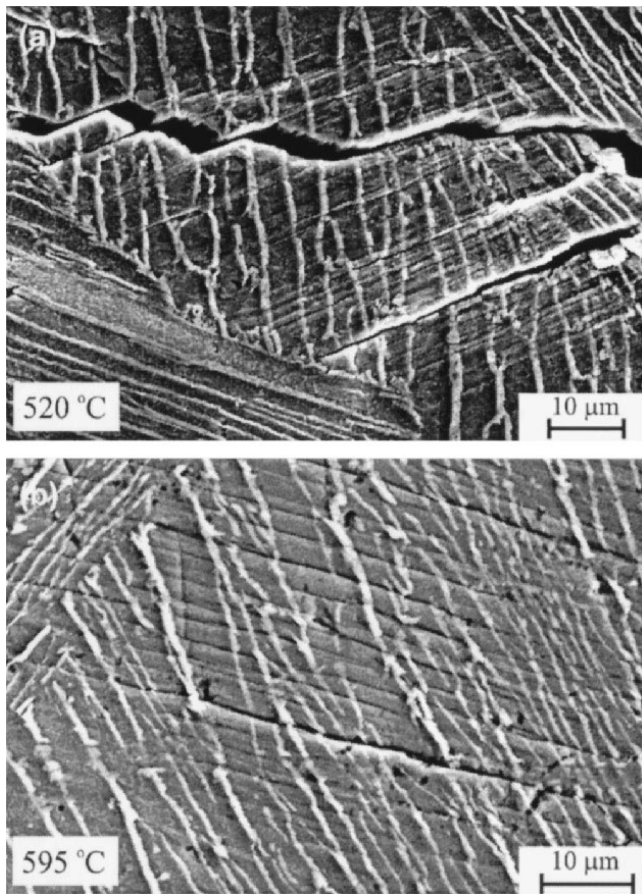


Fig. 11—Planar slip traces at ΔK around $30 \text{ MPa}\sqrt{\text{m}}$ on extra-coarse microstructure tested under 0.05 Hz loading frequency (a) at 520 °C and (b) at 595 °C. Note that slip is more likely restricted within the boundaries of a single colony while the temperature is low.

SEM. The planar nature of fracture in our investigation is also evident by the morphology of the crack path and the cleavage features of the corresponding fracture surface. The planar nature of the slip is usually attributed to the presence of short-range order (SRO) between Ti and Al atoms.^[34] In alloys that contain no SRO, a more homogeneous slip character prevails,^[34,35] and wavy slip patterns are observed at elevated temperatures.^[36] Moreover, the α phase, while softer than the β phase, has a stronger plastic hardening rate, and, as such, the planar slip patterns originating in the α phase would govern the deformation response of the two-phase system.^[35]

In an earlier investigation by Shechtman and Eylon,^[37] who focused on the slip emission at the fatigue crack tip in large colony Ti microstructures, it was found that the crack tip is subjected to two shear modes: one on the α basal plane (0001) and the other on the α prismatic plane $\{10\bar{1}0\}$, with all dislocations on both planes of the $\langle a \rangle$ -type ($\langle 11\bar{2}0 \rangle$). The typical configuration of these dislocations is found to be a pileup at the α/β interfaces, which apply a substantial stress on the interface. The breakdown of the very first barrier enables doubling the pile-up length and the shear band propagates to the end of the colony. Based on these observations, one may consider the possible shear activity associated with transverse and parallel crack path configurations,

as observed in the present study. While assuming perfect Burgers' relationships between α -Ti and β -Ti platelets, the c -axis [0001] of the α phase is aligned with the β platelets' long axis orientation and one prism direction of the α phase coincides with one $\langle 111 \rangle$ direction of the β phase.^[16,38] Consequently, as illustrated in Figure 13(a), shear activities leading to the parallel crack path configuration may be attributed to $\langle a \rangle$ slip in the (01 $\bar{1}$ 0) prism plane or, eventually, to various pyramidal $\langle c + a \rangle$ slips. On the other hand, shear leading to the transverse crack path, which could not coincide with (01 $\bar{1}$ 0) prism slip, may be relevant to shear activities along (0001) basal slip, (10 $\bar{1}$ 0) prism slip, or, eventually, pyramidal slip (Figure 13(b)).

Different investigations^[39,40] have demonstrated in monotonic testing of Ti alloys with an aluminum concentration ≥ 6 pct, that, above 500 °C, pyramidal slip is limited as a deformation mode as compared to basal and prism slips. Moreover, the possibility of slip occurring along any of these prism or basal directions is generally determined by the corresponding critical resolved shear stress (CRSS). The work of Williams *et al.*^[40] on single crystals of Ti-Al alloy containing up to 6.6 pct Al has shown that the CRSS of prism planes is generally lower than that of basal planes, as represented schematically in Figure 14(a). The differences in the CRSS values between these two slip systems, however, decrease as the temperature increases, as seen in this figure. Additionally, Savage *et al.*^[38] have examined the CRSS values of the three $\langle a \rangle$ -type slip directions on both basal and prism planes, in individual α/β colonies of Ti6242Si at room temperature. Results of their microstrain tests, summarized qualitatively in Figure 14(b), indicate that a significantly lower CRSS is obtained along the a_1 [$2\bar{1}\bar{1}0$] and a_2 [$11\bar{2}0$] prism directions, where a_1 and a_2 are shown schematically in Figure 14(c), consequently leading to the easiest slip. It should be emphasized that these two particular slip directions are contained within (01 $\bar{1}$ 0) and (10 $\bar{1}$ 0) shear planes, which were previously shown to lead to parallel and transverse crack paths, respectively. An attempt therefore is made to describe the fatigue cracking mechanisms of Ti6242 alloy by focusing on the shear activity along the possible slip directions, basal and prismatic, which are considered the easiest for slip in the α/β colony.

B. Proposed Model

The influence of the loading frequency and temperature on the slip characteristics of the prism slip is measured by the associated slip density and the resulting variations in the CRSS along the relevant slip direction. Ghonem and co-workers^[41,42] have shown that, in planar slip deformation, the slip line spacing is inversely proportional to the strain rate, which is in turn governed by the loading frequency and test temperature (Figure 15). The higher the value of either of these two parameters, the higher the strain rate and the smaller the slip line spacing. The high slip density leads to higher slip interactions and an increase in the number of cross-slip events. This condition produces an increase of the CRSS of both the a_1 and a_2 prism directions, and, consequently, either a higher applied stress or a larger number of reversed loading cycles is required to achieve dislocation transmission at the α/β interface and into the β phase. It is then assumed that, as the CRSS is raised, the degree of

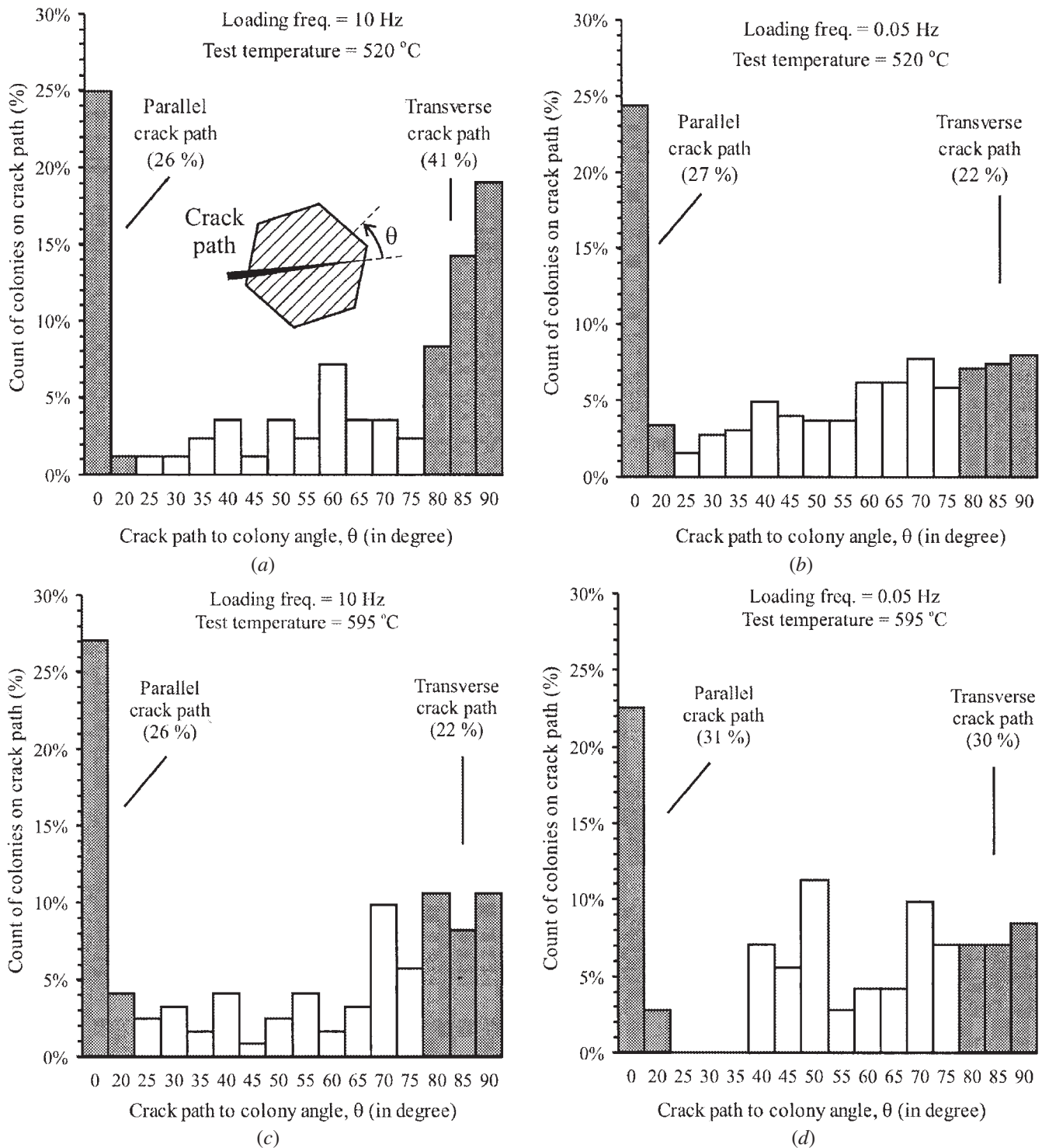


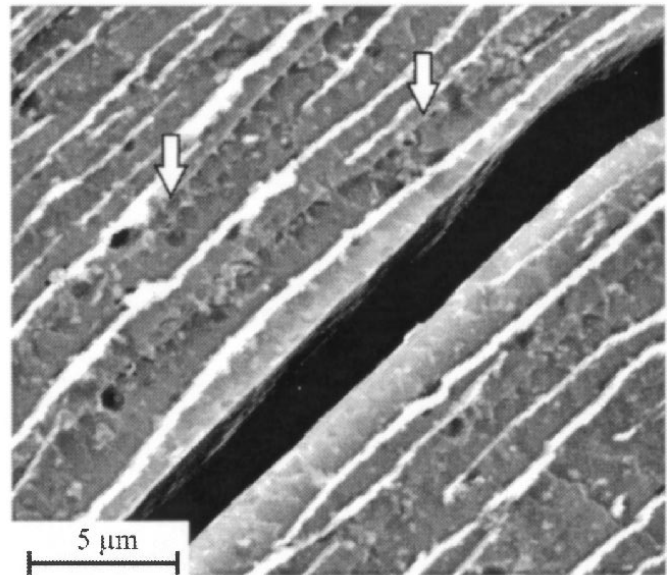
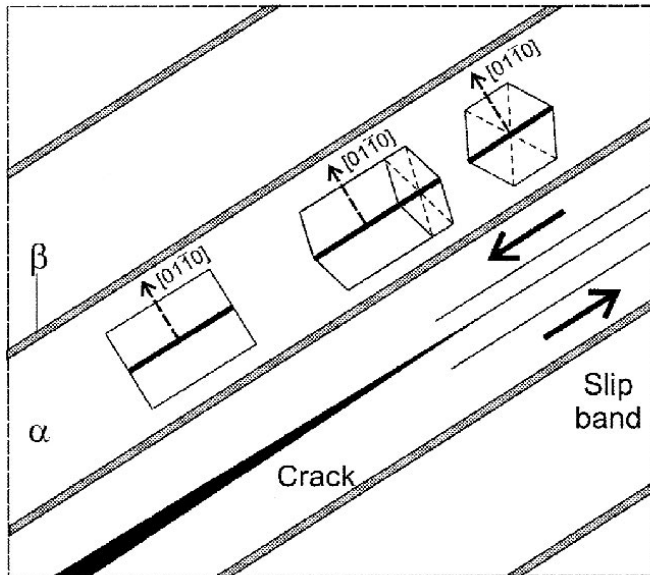
Fig. 12—Crack path direction with respect to long axis colony orientation in transcolony mode of failure. Corresponding test conditions are (a) 10 Hz, 520 °C; (b) 0.05 Hz, 520 °C; (c) 10 Hz, 595 °C; and (d) 0.05 Hz, 595 °C.

deformation anisotropy between a_1 and a_2 is homogenized, thus resulting in a crack path that advances arbitrarily between both slip directions, as illustrated in Figure 16. Conversely, the decrease in the loading frequency would produce lower slip line density, wider slip line spacing, and a decrease of the CRSS of both slip directions. This effect is likely to result in an increased anisotropy between the a_1 and a_2 prism directions as the dislocation transmission at

the α/β interface becomes easier along the a_1 direction. In this condition, the cracking path would be more oriented along the a_1 direction, *i.e.*, quasi-parallel to the α/β interfaces, as shown in the results presented in Figure 12(b).

Similarly, the influence of temperature on the crack growth rate could be explained by considering the associated slip density. Here, the increase in temperature, for the same loading frequency, would produce an increase in the strain rate

(a) Parallel crack path



(b) Transverse crack path

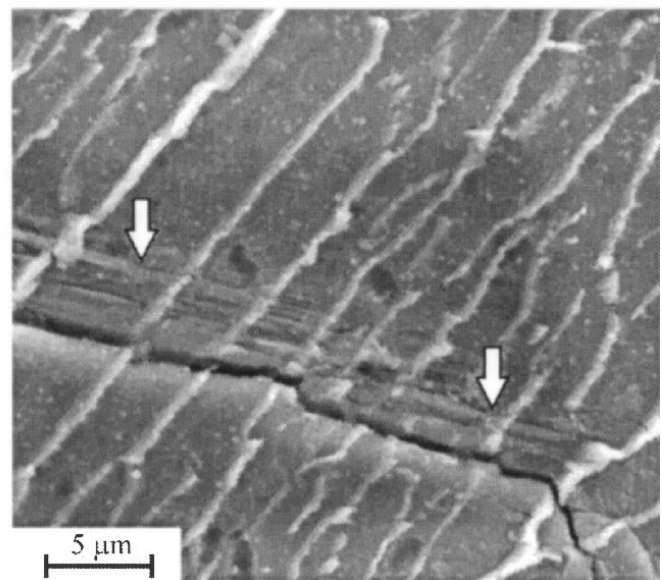
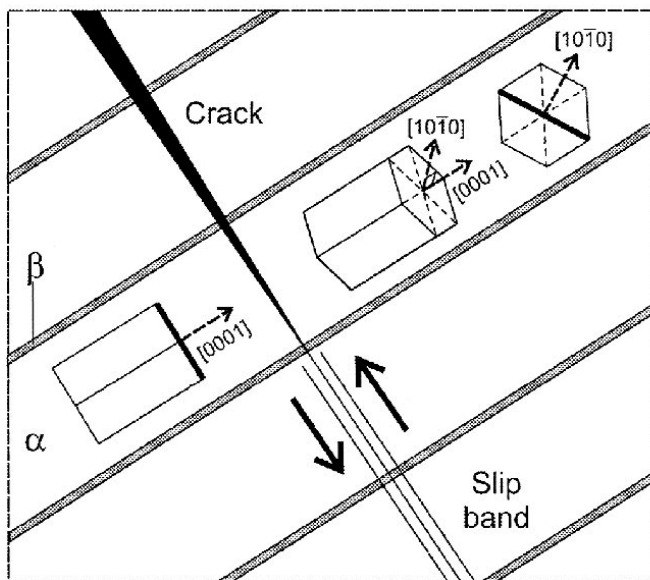


Fig. 13—Schematic relating the orientation of the hcp α -Ti unit cell to (a) parallel crack path and (b) transverse crack path, while colonies are assumed to keep perfect Burgers' relationship between α and β platelets; *i.e.*, the c -axis of α unit cell is parallel to the β lamellae long axis. Arrows on micrographs indicate the presence of slip traces parallel to the crack path.

and consequently an increase in both the slip line density and CRSS of the two slip directions a_1 and a_2 . As such, the higher the temperature, the lower the anisotropy of deformation along these two directions, and the higher the possibility that the cracking path is shared between them. It is also important to note that, as mentioned previously, the increase in temperature makes slip along the basal planes much easier and in turn would increase the possibilities of cracking along the a_2 direction or the direction normal to the α/β interface. The important feature in the higher temperature crack growth is the increase in the slip length along the relevant slip direction due to the relaxation of residual

stresses, particularly at the α/β interface. It is then expected that the crack growth rate be accelerated as the temperature increase, as indicated by the comparison of the crack growth curves in Figures 5 and 6.

C. Effects of Loading Frequency and Temperature

Based on the results given in Figure 12, as well as the preceding discussion, the individual effects of the loading frequency and test temperature on the slip accommodation leading to parallel and transverse crack path configurations are represented schematically in Figure 17. This figure

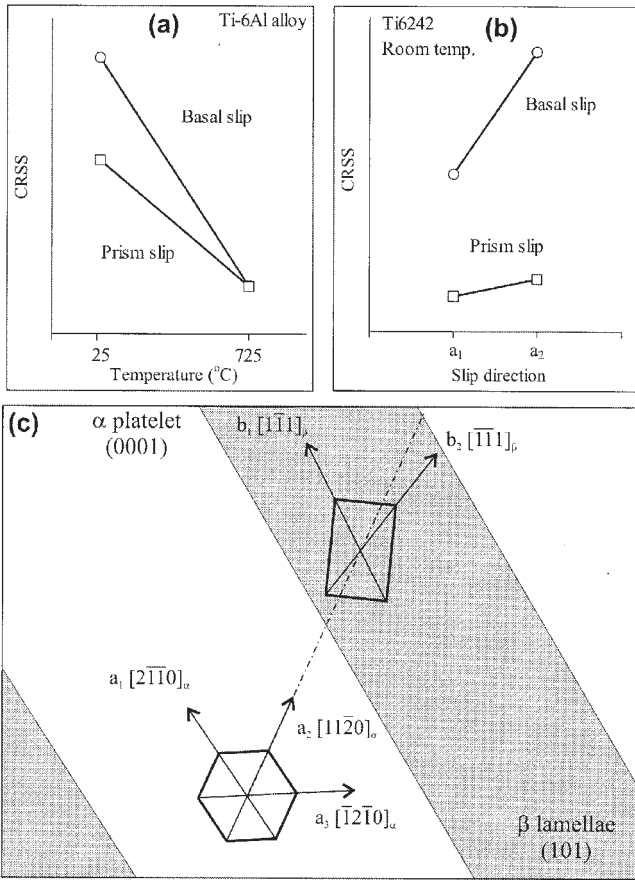


Fig. 14—Evolution of the CRSS in basal and prism slips: (a) in single α phase Ti-6Al as a function of temperature from Williams *et al.*,^[40] (b) at room temperature in two-phase Ti6242 as a function of the slip direction from Savage *et al.*,^[38] and (c) related description of different slip orientations with respect to crystal structure of lamellar titanium alloys.

consists of four domains. Domains I and II correspond to mechanisms observed at the low temperature level. Domain I emphasizes high loading frequency conditions, while domain II is relevant to low frequencies. The role of α/β interfaces on limiting the slip in a_2 prism direction is the controlling deformation mechanism in domain II. At high loading frequency, the role of the interface is limited due to the confinement of the deformation, which is observed to be restricted to a few platelets ahead of the crack tip.^[19] Domains III and IV in Figure 17 correspond to the deformation mechanisms at temperatures near 595 °C. In domain III, the increase of temperature, as previously discussed, makes slip along basal planes easier and, in turn, promotes cracking paths perpendicular to the lamellae, as seen in Figure 12(b). In this regard, the substructure of Ti6242 has been reported which shows that creep behavior at 565 °C is dominated by glide of $\langle a \rangle$ -type cusped dislocations on both basal and prism planes.^[43] Moreover, possibilities of dislocation pileup at the interface are reduced, allowing wavy slip patterns to operate. As a result, the slip anisotropy envisaged at a lower temperature is likely to be inhibited at 595 °C.

The fourth domain describes the effect of hold time at peak stress level appearing when the applied ΔK is larger than $31 \text{ MPa}\sqrt{\text{m}}$. The Irwin's plastic zone size correction

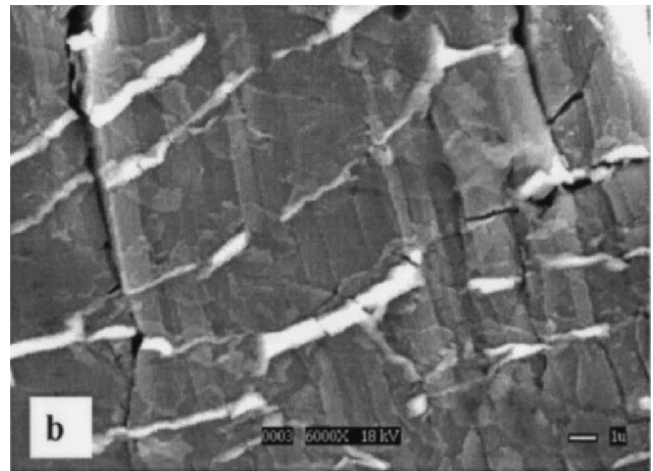
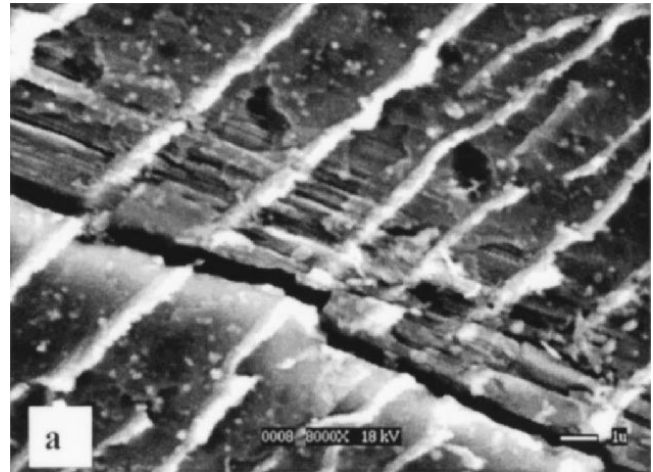


Fig. 15—Slip line appearance along the fracture path in two specimens with two different loading frequencies at 520 °C: (a) 10 Hz and (b) 0.05 Hz.

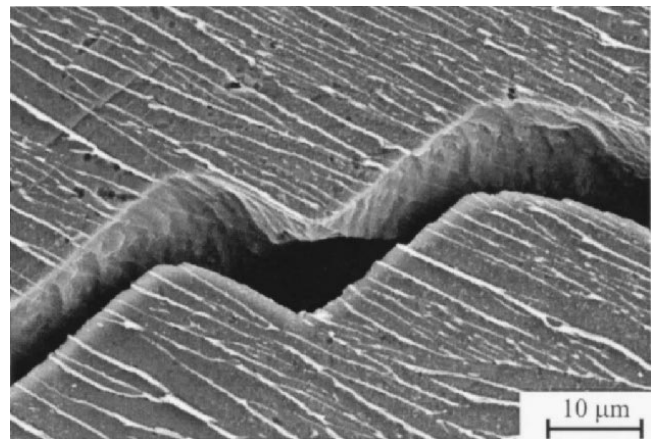


Fig. 16—The homogenized deformation anisotropy of a_1 and a_2 slip at high frequency (10 Hz, 520 °C) results in a crack path that advances arbitrarily along both slip directions.

corresponding to this ΔK amplitude is equal to $427 \mu\text{m}$ in plane strain conditions, which suggests that the plastic zone size is large enough to encompass at least one α/β colony, as seen in Figure 2(a). Under this condition, the spread of

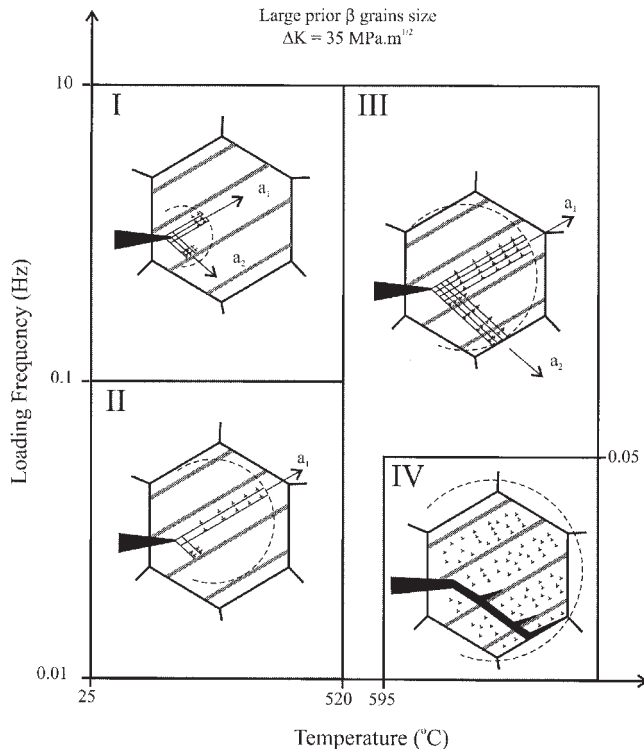


Fig. 17—A fracture path map illustrating the role of loading frequency and temperature on the crack-tip slip process at α/β interfaces. The arrows represented near the crack tip indicate the predominant crack path direction.

the time-dependent plastic zone is of a comparable size to the average colony size and leads to interboundary fracture. This could be interpreted by the extent of creep flow allowing the relaxation of dislocation pileup across internal boundaries.^[9,10,11,14] When a hold time is imposed at peak stress at 595 °C, dislocation transfer occurs easily through the α/β interfaces and intercolony boundaries, and pileup occurs at prior β grain boundaries. The dependence of this regime on the microstructure is analyzed in Section D.

D. Effects of Microstructure

In domain IV, the intergranular fracture is controlled by the prior β grain size. Therefore, fine-grain microstructures will reach intergranular fracture at a stress level lower than that corresponding to coarse-grain microstructures. This could explain the difference in crack growth rate of coarse and extra-coarse microstructures when a hold time is imposed (Figure 6), since the coarse microstructure has a relatively larger prior β grain size, as seen in Figure 2(a). In the domains relative to quasi-cleavage fracture, it appears, as discussed previously, that the microstructure has little influence on the crack-tip slip process except in domain II, which is affected by the decrease of slip along the a_2 direction across the α/β interfaces. It was found in domain II that the fine microstructure exhibits FCGRs than the extra-coarse microstructure, accompanied by a plateau of FCGRs. This result is in line with data by Williams and Luetjering,^[44] who show that, on aged Ti-6Al-4V tested at room temperature, the fine/coarse microstructure difference is more significant if the microstructure is lamellar rather than equiaxed. In the present study, however, it is observed that the

difference in the FCGR at the low ΔK levels disappeared at 595 °C. Ruppen and McEvily^[31] have noticed that the presence of plateau effects is more pronounced at 540 °C than at room temperature in Ti6242, but did not detect a notable effect of microstructure. In addition, these authors have observed that the plateau of fatigue crack growth rates disappears under vacuum conditions, which suggests combined environment/microstructure effects. The appearance of quasi-cleavage facets, which dominates the fracture surface in all testing conditions, suggests that the accelerated formation of the facets is likely due to oxygen diffusion at the crack tip.^[45] A complex interaction could then exist between the depth of oxygen diffusion and the crack-tip cyclic zone size. Consequently, microstructure morphology, particularly the lamella size, as well as the loading frequency and test temperature, would directly influence these two parameters. The full understanding of the role of each of these parameters on the enhancement of the diffusion-assisted crack growth process could be achieved through the computational investigation of the cracking mechanisms in the α/β colony.

V. CONCLUSIONS

Fatigue crack growth experiments were carried out on three fully lamellar microstructures of Ti6242 alloy at two temperatures, 520 °C and 595 °C, for the loading frequencies of 10 and 0.05 Hz. The latter frequency was examined with and without 300-second hold time. All the tests were performed in air environment and at a stress ratio of 0.1. Major results of this study can be summarized as follows.

1. At 520 °C, the FCGR at 10 Hz is not significantly influenced by changes in the microstructure. This behavior also exists for the 0.05 Hz at ΔK higher than 30 MPa \sqrt{m} . At lower ΔK , the FCGR is higher in the fine lamellar microstructure and is accompanied by the appearance of a plateau, which disappears in the extra large lamella microstructure. This plateau effect was viewed as a result of environment/microstructure interactions. Furthermore, the addition of a 300-second hold time at peak stress does not alter the crack growth behavior, which tends to indicate that creep strain effects at 520 °C are limited in this process.
2. At 595 °C, while the general level of the FCGR is higher than that of 520 °C, effects of the loading frequency and hold time remain approximately similar to that at the lower temperature level. Unlike results at 520 °C, the FCGR at low ΔK is not influenced by variations in lamellar microstructure. Substantial crack growth, however, occurs at ΔK higher than 31 MPa \sqrt{m} , particularly in the presence of hold time. At this ΔK and higher levels, the fracture failure is dominated by prior β intergranular fracture and α/β interface decohesion.
3. Under all test conditions, the fatigue process is predominantly controlled by one single mechanism related to transcolony fracture associated with the formation of quasi-cleavage facets, which are oriented along heavily sheared slip bands. An equal tendency for near-0 deg and near-90 deg angle crack paths is observed at high frequency. These angles are measured with respect to

the lamellae long-axis direction. At low frequency, a significant reduction for crack paths at near-90 deg angle, and predominance for paths parallel to the platelets, is detected at 520 °C. This phenomenon seems almost absent at 595 °C.

4. The fatigue crack growth results and the associated fracture behavior as obtained in this study are rationalized in terms of the crack-tip slip process. It is proposed that the reduction of a_2 prism slip with the decrease in the loading frequency plays a significant role in the decrease of perpendicular-to-lamellae crack paths at 520 °C. In addition, the decrease of the loading frequency results in diminishing the homogeneity and density of the slip at the crack tip, which tends to reduce interactions between adjacent slip planes. The lack of cross-slip causes a decrease of CRSS for macroscopic plastic flow and softening in both a_1 and a_2 prism directions, which leads to higher crack growth rates. At 595 °C, the increase of temperature reduces the anisotropy of slip transmission at the α/β interfaces and further promotes cracking of the basal plane along a direction perpendicular to the α/β interface.

ACKNOWLEDGMENTS

The financial and material support of this study was made possible by SNECMA, Etablissement de Villaroche (Moissy Cramayel, France). Dr. Jean-Yves Guedou, the program monitor at SNECMA, is gratefully acknowledged.

REFERENCES

1. R.R. Boyer: *Mater. Sci. Eng.*, 1996, vol. A213, pp. 103-14.
2. D. Eylon, J.A. Hall, C.M. Pierce, and D.L. Ruckle: *Metall. Trans. A*, 1976, vol. 7A, pp. 1817-26.
3. R.R. Boyer and G. Lütjering: in *Advances in the Science and Technology of Titanium Alloy Processing*, I. Weiss, R. Srinivasan, P.J. Bania, D. Eylon, and S.L. Semiatin, eds., TMS, Warrendale, PA, 1997, pp. 349-67.
4. G. Lütjering: *Mater. Sci. Eng.*, 1998, vol. A243, pp. 32-45.
5. G.R. Yoder, L.A. Cooley, and T.W. Crooker: *J. Eng. Mater. Technol. Trans. ASME*, 1977, vol. 99 (4) pp. 313-18.
6. C.C. Chen and J.E. Coyne: in *Titanium '80*, H. Kimura and O. Izumi, eds., TMS-AIME, Warrendale, PA, 1980, vol. 2, pp. 1197-1207.
7. N.R. Moody and W.W. Gerberich: *Met. Sci.*, 1980, Mar., pp. 95-100.
8. J.K. Gregory: in *Handbook of Fatigue Crack Propagation in Metallic Structures*, A. Carpinteri, ed., Elsevier Science, Amsterdam, 1994, pp. 281-322.
9. H. Ghonem and R. Foerch: *Mater. Sci. Eng.*, 1991, vol. A138, pp. 69-81.
10. R. Foerch, A. Madsen, and H. Ghonem: *Metall. Trans. A*, 1993, vol. 24A, pp. 1321-32.
11. A.H. Rosenberger and H. Ghonem: *Fatigue Fract. Eng. Mater. Struct.*, 1994, vol. 17 (4), pp. 397-410.
12. B.K. Parida and T. Nicholas: *Fatigue Fract. Eng. Mater. Struct.*, 1994, vol. 17 (5), pp. 551-61.
13. S. Lesterlin, C. Sarrazin-Baudoux, and J. Petit: *Scripta Mater.*, 1996, vol. 34 (4), pp. 651-57.
14. W.H. Miller Jr., R.T. Chen, and E.A. Starke, Jr.: *Metall. Trans. A*, 1997, vol. 18A, pp. 1451-68.
15. P.J. Bania and J.A. Hall: in *Titanium '84*, TMS-AIME, Warrendale, PA, 1984, pp. 2371-78.
16. J.A. Ruppen and A.J. McEvily: in *Fractography and Materials Science*, ASTM STP 733, L.N. Gilbertson and R.D. Zipp, eds., ASTM, Philadelphia, PA, 1981, pp. 32-50.
17. Z. Song and D.W. Hoepfner: *Int. J. Fatigue*, 1988, vol. 10 (4), pp. 211-18.
18. J.C. Chesnutt and N.E. Paton: in *Titanium '80*, H. Kimura and O. Izumi, eds., TMS-AIME, Warrendale, PA, 1980, vol. 3, pp. 1855-63.
19. W.J. Evans and C. Gostelow: *Metall. Trans. A*, 1979, vol. 10A, pp. 1837-46.
20. A.W. Sommer and D. Eylon: *Metall. Trans. A*, 1983, vol. 14A, pp. 2178-81.
21. D. Eylon and J.A. Hall: *Metall. Trans. A*, 1977, vol. 8A, pp. 981-90.
22. L.S. Vesier and S.D. Antolovich: *Eng. Fract. Mech.*, 1990, vol. 37 (4), pp. 753-75.
23. P.J. Bania and D. Eylon: *Metall. Trans. A*, 1978, vol. 9A, pp. 847-55.
24. C.A. Stubbington and S. Pearson: *Eng. Fract. Mech.*, 1978, vol. 10, pp. 723-855.
25. F.S. Lin, E.A. Starke, Jr., S.B. Chakraborty, and A. Gysler: *Metall. Trans. A*, 1984, vol. 15A, pp. 1229-46.
26. J. Wegmann, G. Albrecht, K.D. Lütjering, Folkers, and C. Liesner: *Z. Metallkd.*, 1997, vol. 88 (10), pp. 764-72.
27. K.S. Ravichandran: *Acta Metall. Mater.*, 1991, vol. 39 (3), pp. 401-10.
28. K.S. Chan, C.C. Wojcik, and D.A. Koss: *Metall. Trans. A*, 1981, vol. 12A, pp. 1899-907.
29. S. Suri, G.B. Viswanathan, T. Neeraj, D.H. Hou, and M.J. Mills: *Acta Mater.*, 1999, vol. 47 (3), pp. 1019-34.
30. M. Es-Soumi: *Mater. Characterization*, 2000, vol. 45, pp. 153-64.
31. J.A. Ruppen and A.J. McEvily: *Fatigue Fract. Eng. Mater. Struct.*, 1979, vol. 2, pp. 63-72.
32. G.R. Yoder, L.A. Cooley, and T.W. Crooker: *J. Eng. Mater. Technol.*, 1977, October, pp. 313-18.
33. I.W. Hall and C. Hammond: *Mater. Sci. Eng.*, 1978, vol. 32, pp. 241-53.
34. T. Neeraj and M.J. Mills: *Mater. Sci. Eng.*, 2001, vols. 319-321, pp. 415-19.
35. A.S. Beranger, X. Feaugas, and M. Clavel: *Mater. Sci. Eng.*, 1993, vol. A172, pp. 31-41.
36. J.C. Williams, A.W. Sommer, and P.P. Tung: *Metall. Trans.*, 1972, vol. 3, pp. 2979-84.
37. D. Shechtman and D. Eylon: *Metall. Trans. A*, 1978, vol. 9A, pp. 1018-20.
38. M.F. Savage, J. Tatalovich, M. Zupan, K.J. Hemker, and M.J. Mills: *Mater. Sci. Eng.*, 2001, vols. A319-A321, pp. 398-403.
39. G. Welsch and W. Bunk: *Metall. Trans. A*, 1982, vol. 13A, pp. 889-99.
40. J.C. Williams, R.G. Baggerly, and N.E. Paton: *Metall. Mater. Trans. A*, 2002, vol. 33A, pp. 837-50.
41. D. Zheng, A. Rosenberger, and H. Ghonem: *Metall. Trans. A*, 1992, vol. 23a, pp. 3067-72.
42. H. Ghonem and D. Zheng: *Mater. Sci. Eng.*, 1993, vol. A161, pp. 13-21.
43. G.B. Viswanathan, S. Karthikeyan, R.W. Hayes, and M.J. Mills: *Metall. Mater. Trans. A*, 2002, vol. 33A, pp. 329-36.
44. J.C. Williams and G. Luetjering: in *Titanium '80*, H. Kimura and O. Izumi, eds., TMS-AIME, Warrendale, PA, 1980, vol. 1, pp. 671-81.
45. G.T. Gray III, G. Luetjering, and J.C. Williams: *Metall. Mater. Trans. A*, 1990, vol. 21A, pp. 95-105.